NJC

ROYAL SOCIETY OF CHEMISTRY

PAPER

View Article Online
View Journal | View Issue

Cite this: *New J. Chem.*, 2024, **48**, 4030

Synthesis and real structure of RUB-11, a novel high-density silica zeolite based on magadiite layers†

Isabel Grosskreuz, [a] Yaşar Krysiak, [bc] Hermann Gies, [a] Enrico Mugnaioli[d] and Bernd Marler*[a]

The discovery of new zeolite framework types plays an important role in producing new porous materials for applications such as adsorption, catalysis, separation, *etc.* RUB-11, a new all-silica zeolite with high density (2.11 g cm^{-3}), was synthesised at 160 °C from reaction mixtures consisting of SiO_2/ethylenediamine/H_2O in a xenon atmosphere of 30 bar for a long reaction time (140 d). Physico-chemical characterisation using solid-state NMR spectroscopy, SEM, TG-DSC and ATR-FTIR spectroscopy confirmed that RUB-11 is a framework silicate. The atomic structure was solved by 3D electron diffraction using the fast-automated diffraction tomography method. The structure model of monoclinic symmetry with lattice parameters of a_0 = 7.3929(5) Å, b_0 = 7.3942(3) Å, c_0 = 26.1786(13) Å and β = 98.372(7)° (space group: *Pc*) was refined against electron diffraction data (dynamical refinement) and powder diffraction data. An additional distance-least-squares refinement confirmed the feasibility of forming a stress-free silica framework of RUB-11 topology. The chemical composition of RUB-11 per unit cell is 30 SiO_2. The framework silicate RUB-11 is structurally closely related to layer silicate magadiite and can be regarded as an interlayer expanded zeolite (IEZ) based on magadiite-type layers. Both materials contain topologically identical, dense layers, named mag layers. In the case of RUB-11, these layers are interconnected *via* additional silicon atoms leading to a complete framework with a 2-dimensional pore system consisting of intersecting 8-ring channels. The synthesis route leading to RUB-11 is in contrast to typical IEZs, which are obtained in a two-step process. According to the electron diffraction data and the XRD powder patterns, RUB-11 has a disordered structure. A detailed analysis revealed that two different types of disorder concerning the stacking of layer-like building units (consisting of mag layers plus interconnecting silicon atoms) contribute to the real structure of RUB-11. It is surprising that the channel-like pores of RUB-11 are completely empty when separated from the reaction mixture.

Received 22nd July 2023,
Accepted 25th January 2024

DOI: 10.1039/d3nj03424k

rsc.li/njc

1 Introduction

Zeolites have been known for a long time and are widely used in the industry as ion exchangers, adsorbents, catalysts and catalyst supports.[1–3] Their crystalline structures consist of three-dimensional frameworks constructed from 4-connected [TO_4]-tetrahedra in three dimensions. The frameworks are characterised by uniform pore sizes and pore openings of $<$20 Å able to take up water or hydrocarbon molecules whose size is equal to or less than the size of the pore openings. The composition of the tetrahedral frameworks can vary considerably with tetravalent metal atoms (*e.g.*, Si, Ge, Ti, and Zr) or trivalent atoms (*e.g.*, Al, Ga, B, and Fe) located in the centers of the tetrahedra. If a mixture of tetravalent and trivalent atoms (*e.g.*, Si and Al) occupies the T sites of the framework, the framework is anionic and non-framework cations such as alkali or alkaline earth metal cations or organic cations have to balance the negative charge. In the case of protons as charge balancing species, complex silicic acids are formed. If, however, only silicon occupies the T sites, the framework is neutral and,

[a] *Institute of Geology, Mineralogy and Geophysics, University of Bochum, Universitaetsstrasse 150, D-44801 Bochum, Germany. E-mail: bernd.marler@rub.de; Fax: +49 0234 32 14433; Tel: +49 2332 665580*
[b] *Department of Structure Analysis, Institute of Physics, Czech Academy of Sciences, Cukrovarnická 10/112, CZ-17000 Prague, Czech Republic*
[c] *Institute of Anorganic Chemistry (ACI), Leibniz University Hannover (LUH), Callinstraße 9, Building 2501, Room 189, D-30167 Hannover, Germany*
[d] *Instituto Italiano di Tecnologia, Center for Nanotechnology Innovation, NEST, Piazza San Silvestro 12, I-56127 Pisa, Italy*

† Electronic supplementary information (ESI) available. CCDC 2278560. For ESI and crystallographic data in CIF or other electronic format see DOI: https://doi.org/10.1039/d3nj03424k

typically, the material is hydrophobic and thermally stable up to a very high temperature (approx. 1000 °C). Pure silica frameworks are useful in absorption and separation processes of liquids and gases and may serve as catalyst supports.

Currently, there are 256 ordered microporous framework structures of different topologies as listed by the *International Zeolite Association*.[4,5] In addition, there are 29 families of disordered zeolites.[4] Each structure has unique pore sizes, channel cross-sections and cage dimensions that lead to particular properties.

The discovery of new zeolite framework types plays an important role in producing new catalytically active materials. Reactions like the interlayer expansion and topotactic condensation of layered silicates as precursors yield several new framework types. Still, the demand for novel structures possessing a new framework topology and, thus, different properties than those of known materials, is on the rise. Any new zeolite has the potential to improve the performance over those materials presently in use.

More recently, so called interlayer expanded zeolites (IEZs)[6–8] have been synthesised. These frameworks expand the spectrum of microporous materials offering reactive sites as a part of the interrupted framework, which can be modified post-synthesis.[9] So far, IEZs, nearly exclusively, have been obtained in a two-step process: synthesis of a layer silicate and pillaring the silicate layers of the precursor with covalently bonded SiX4 units by a second hydrothermal synthesis.

There is an interesting exception to this typical synthesis procedure: the synthesis of RUB-5 that can be regarded as the interlayer expanded zeolite (IEZ) based on silicate layers, which are known from layer silicates RUB-6 and kenyaite.[10–12] RUB-5 is an IEZ being formed in a one-step hydrothermal synthesis and, moreover, possesses a fully 4-connected SiO_2 framework. The close relationship between RUB-5 and RUB-11 will be presented in the Results and discussion (section 3) section.

Disorder is frequently observed in HLSs, zeolites, IEZs and related materials. In particular, stacking disorder of layer-like building units (LLBUs) is common and leads to polymorphism with distinct ordered endmember structures. A disordered arrangement of LLBUs can be quickly identified by anisotropic broadening of X-ray diffraction peaks.

Due to the generally weak interactions between neighbouring silicate layers, stacking disorder is a typical concomitant phenomenon when crystallising HLSs. Details on HLSs (often also named ''2D zeolites'') can be obtained from the *Database of Hydrous Layer Silcates*.[12] The structure of zeolite beta, consisting of interconnected LLBUs, is the classical example of a highly disordered zeolite which is directly obtained by hydrothermal synthesis.[13,14] Nearly, all IEZs exhibit a disordered structure.[15–17] Also, microporous materials obtained by a condensation reaction applied to an HLS precursor are often of poor crystallinity. Usually, stacking disorder, which is already present in the precursor, will be retained by the condensed product.[18] All these materials predominantly consist of very small crystallites.

Anisotropic peak broadening, poor crystallinity and very small crystals evoke a predicament for structure solution methods. Although the scientific progress of combining X-rays, 3D electron diffraction and electron microscopy has taken a leap in recent years, it is still a challenge to solve the structure of a severely disordered and very fine-grained material.

Here, we present the synthesis, characterisation and crystal structure of a new high density silica zeolite, which can also be considered to represent an unusual IEZ. The structure of RUB-11 remained unknown for a long time due to very thin crystals (0.1 μm) and severe disorder. Ultimately, powder diffraction methods failed and the average structure could only recently be solved using a 3D electron diffraction technique. In addition, the real structure of RUB-11 and the nature of the disorder were analysed thoroughly by electron diffraction and supported by the simulation and comparison of X-ray powder diagrams.

2 Experimental section

2.1 Synthesis

RUB-11 was synthesised at 160 °C from a reaction mixture of 1 SiO_2/1 ethylenediamine/55.5 H_2O in a xenon atmosphere. Tetramethoxysilane (>98%, Fluka) was added drop-wise to a vigorously stirred 1 molar aqueous solution of ethylenediamine (99%, Merck). Tetramethoxysilane was hydrolysed during this process to form fresh silicic acid and methanol. Methanol was not removed prior to the hydrothermal synthesis. This reaction mixture was filled in an autoclave, which possessed a valve for additional gas feed. Subsequently, xenon gas was added to a pressure of 30 bar (at room temperature). This composition was kept in an oven under static conditions for 140 d.

The synthesis was performed to produce a xenon containing clathrasil, and did not aim for the crystallisation of a new phase.

As can be seen from Table 1, xenon is not essential to produce RUB-11; on the other hand, the xenon gas also does not obstruct the synthesis of RUB-11.

After heating, the solid products were separated from the mother liquid, washed with ethanol and distilled water and dried overnight at room temperature. The reaction product (see Table 1) contained RUB-11, xenon-dodecasil 3C (MTN), xenon-melanophlogite (MEP), silica-ZSM-22 (TON) and cristobalite, which were separated from each other by hand picking of crystals and crystal aggregates under an optical microscope. A small amount of xenon-dodecasil 3C (abbreviated as Xe-D3C) remained as an impurity.

Additional synthesis experiments in a wider temperature range (150–200 °C) had been performed using methylamine (40% in water, Fluka) instead of ethylenediamine to prepare reaction mixtures of SiO_2/methylamine/H_2O and using silica glass ampules as reaction vessels.[19] Four different silica sources were used: tetramethoxysilane (>98%), silica gel (high-purity grade, Merck), precipitated silica (purissima, Merck) and

Table 1 Synthesis of RUB-11 (MA: methylamine, ED: ethylenediamine, *: aerosil, +: tetramethoxysilane)

Synthesis			
Comp. of the react. mixture	Temp.	Time	Crystalline products
3.9 SiO_2*/21.5 MA/55.5 H_2O[19]	150 °C	214 d	MTN, (TON)
	160 °C	214 d	MTN, TON, crist.
	170 °C	214 d	MTN, TON, RUB-11, crist.
	180 °C	214 d	TON, MTN, RUB-11 (MEP)
	200 °C	214 d	MTN, RUB-11
1.0 SiO_2^+/1.0 ED/55.5 H_2O (+30 bar xenon)	160 °C	140 d	MTN, RUB-11, TON, MEP

fumed silica (AEROSIL 400, degussa). In all cases, a mixture of crystalline materials was obtained (see Table 1).

2.2 General characterisation

2.2.1 SEM. Scanning electron micrographs were taken using a Zeiss Merlin Gemini 2 electron microscope to study the morphology of the crystals and the homogeneity of the samples. The samples were gold coated by vacuum vapour deposition prior to analysis. The voltage was set to 5 kV.

Further scanning electron microscopy was performed with a Hitachi Regulus SU8200 system. Powdered samples were fixed on carbon adhesive tape. The voltage was set to 10 kV with an emission current of 10 900 nA at a working distance of 9 mm.

2.2.2 EDX. For semi-quantitative chemical analysis, EDX measurements were performed using a Hitachi Regulus 8230 system with an Oxford UltiMAX 100 in mapping mode. The voltage and working distance were set to 10 kV and 9.1 mm, respectively. The weak aluminum external signal originates from the sample carrier.

2.2.3 TA. The thermal properties of the as-synthesised material were investigated by simultaneous DSC/TG measurements using a TA Instruments SDT650 thermal analyzer. The sample was heated in synthetic air from 30 to 1200 °C at a heating rate of 10 °C min^{-1}.

2.2.4 FTIR. Fourier transform infrared spectroscopy (FTIR-ATR) was performed using a Nicolet 6700 FT-IR spectrometer equipped with a Smart Orbit Diamond ATR unit. The spectra of the pure samples were recorded in dry air between 350 and 4000 cm^{-1} with a resolution of 4 cm^{-1}.

2.2.5 NMR. Solid state NMR MAS spectra were recorded at room temperature with a Bruker ASX-400 spectrometer using standard Bruker MAS probes. In order to average the chemical shift anisotropies, samples were spun about the magic angle. Tetramethylsilane (TMS) was used as a chemical shift standard. Recording conditions are listed in Table S1 in the ESI.† ^{29}Si hpdec MAS NMR measurements were performed in order to record quantitative intensities.

2.2.6 3D electron diffraction. Powdered samples were dispersed in ethanol using an ultrasonic bath and dropped on a carbon-coated copper grid. Transmission electron microscopy (TEM) measurements were carried out with a TEM FEI Tecnai 20 equipped with a LaB_6 cathode, working at 200 kV. TEM images and nanoelectron diffraction (NED) patterns were recorded with a CCD camera (14-bit 2048 × 2048 pixel Olympus Veleta) using an Olympus iTEM software. A condenser aperture of 10 μm and mild illumination settings (spot size 6) were used in order to produce a semi-parallel beam of 1380 nm in diameter on the sample (0.05 e^- $Å^{-2}$ s^{-1}). The 3D ED data were collected using the acquisition module Fast-ADT (fast and automated diffraction tomography, FADT)[20] using the authors own developed scripts in the Olympus Soft Imaging Solutions iTEM software. The total accumulated electron beam dose including tracking was approximately 9 e^- $Å^{-2}$ per data set. The NED data were collected with electron beam precession (precession electron diffraction, PED) in order to improve reflection intensity integration quality.[21,22] PED was performed using a Digistar unit developed by NanoMEGAS SPRL. The precession angle was kept at 1°. The PETS2.0 software package[23] was used for 3D ED data processing. The structure was determined *ab initio* assuming the kinematic approximation $I \sim |Fhkl|^2$ in reciprocal space using Direct Methods as implemented in the program SIR2014.[24] Scattering factors for electrons were taken from Doyle and Turner.[25] Difference Fourier mapping and least-squares (dynamical) refinement were performed with the software JANA2006.[26]

2.2.7 PXRD. Powder XRD data were recorded using a Siemens D5000 powder diffractometer in modified Debye–Scherrer geometry using CuKα_1 radiation (λ = 1.54059 Å). The sample was loaded onto a borosilicate glass capillary (0.3 mm in diameter) to avoid a preferred orientation of the crystals. The diffractometer was equipped with a curved germanium (111) primary monochromator and a Braun linear position-sensitive detector (2θ coverage = 6°). The Rietveld refinement of the average structure of RUB-11 later revealed that the sample contained 1.06(4)% Xe-D3C (see below).

2.2.8 Rietveld refinements. For a structure refinement of the average structure, the program FullProf was used on PXRD data.[27] The refinement was performed with soft distance restraints: d(Si–O) = 1.62(1) Å, d(Si···Si) = 3.08(4) Å, and d(O···O) = 2.62(3) Å. To fit the anisotropic half-widths of the reflections, nine additional parameters had to be used. Moreover, specific small values for the half-widths of the three strong reflections ($\bar{4}02$), (023) and (202) had to be applied (for details see also Section 3.3).

2.2.9 DLS refinements. Distance-least-squares refinements were conducted using the DLS-76 program.[28] For the optimisation, a Si–O distance of 1.610 Å, a Si···Si distance of 3.080 Å and

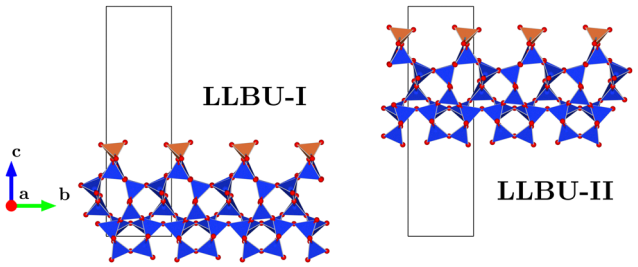

Fig. 1 The layer-like building units used to model the disordered structure of RUB-11. Structure models have been plotted using the program VESTA.[32]

an O···O distance of 2.625 Å were assumed as the typical features of high silica zeolites.

2.2.10 Disorder modeling to reveal the real structure. After determining the average structure of RUB-11, the disordered real structure was studied by single crystal electron diffraction and powder XRD. Experimental and simulated powder patterns were compared using the program DIFFaX.[29] In order to explain the diffuse scattering in ED patterns and simulate broadened reflections in the XRD powder diagram, stacking disordered structures based on two different types of a disordered arrangement of layer-like building units (LLBUs) were modeled. The ordered (average) structure of RUB-11 was separated into two layers extending along *a* and *b* directions. These LLBUs, termed as LLBU-I and LLBU-II, consist of either mag layer type I or mag layer type II, plus an interconnecting silicon atom. The two layer types, as well as the LLBUs, are enantiomorphic to each other. The structures of RUB-11 and magadiite differ with respect to the interconnecting tetrahedron, which is missing in magadiite (see Fig. 1, 9 and 10). The symmetry of the layers corresponds to the plane space group $C21(1)$.[30]

The program FAULTS,[31] the successor of DIFFaX,[29] has been used to simulate a diffraction pattern with the parameter values as shown in Table S2 in the ESI.† DIFFaX and FAULTS simulations are very sensitive to the type and degree of disorder, and a thorough preparation of a meaningful starting model is, therefore, necessary. The obtained simulated PXRD pattern has then been refined against the experimental PXRD pattern by the Levenberg Marquard Minimisation Algorithm using FAULTS.[31] After adding a linear interpolation of background points, the scale factor of both phases, RUB-11 and the small impurity phase Xe-D3C, the zero shift, and Pseudo-Voigt profile function parameters have been refined. The program, however, does not allow for a refinement of asymmetry parameters which, unfortunately, has a significant impact on the shape (but not on the integrated intensity) of the first strong peak of the PXRD pattern. Finally, transition probabilities and shift vectors between successive layers have been refined.

3 Results and discussion

3.1 Synthesis

The synthesis experiments led to the crystallisation of mixtures of four different microporous phases: RUB-11, silica-ZSM-22 (zeolite framework type TON), Xe-D3C (MTN), xenon-melanophlogite (MEP), and cristobalite (crist.) (see Table 1).

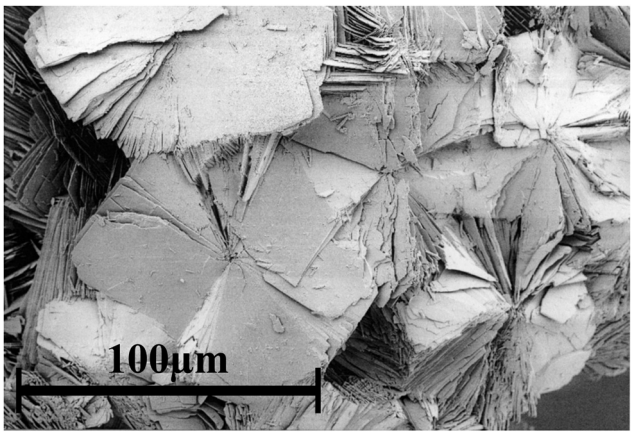

Fig. 2 SEM micrograph of plate-like aggregates of RUB-11 crystals.

The phases were identified by X-ray powder diffraction. No synthesis run produced pure RUB-11. The crystallisation proceeded very slowly. In the case of methylamine (MA) as the organic additive, complete crystallisation was only achieved at 200 °C within a synthesis time of 214 d. Using ethylenediamine (ED), the crystallisation was complete after 140 d. The varying silica sources used to prepare the reaction mixture had no significant impact on the composition of the reaction product.

An optical microscope was sufficient to distinguish and separate the different product phases due to characteristic morphologies: RUB-11 as aggregates of small plates, silica-ZSM-22 as elongated prisms (TON), Xe-D3C as intergrown octahedra (MTN) and xenon-melanophlogite as cubes (MEP).

Fig. S1 (ESI†) shows the typical morphologies of RUB-11 aggregates and Xe-D3C crystals as seen under an optical microscope. It was, however, impossible to perfectly separate RUB-11 from Xe-D3C, since, in a few cases, an intergrowth of RUB-11 aggregates and crystals of the impurity phase was not recognised.

For a detailed characterisation of RUB-11, the sample synthesised under an xenon atmosphere was used.

3.2 Properties of RUB-11

SEM. RUB-11 consists of very thin, colorless crystals, which are intergrown to form sphere-like aggregates (Fig. 2). The individual plate-like crystals are approx. 20–30 µm in diameter with a thickness of about 0.1 µm. The plates seem to crystallise with a rectangular shape.

EDX. Fig. S2 (ESI†) displays the EDX spectrum of a RUB-11 crystal providing a qualitative chemical analysis, which revealed the presence of silicon and oxygen exclusively. No xenon was detected (see also Fig. S2, ESI†). Since small amounts of carbon and nitrogen are difficult to detect by EDX, no statement on these elements can be given. The thermal analysis and the FTIR spectrum, however, showed RUB-11 to be free of carbon and nitrogen. As the synthesis mixture contained only silica as a potential framework building compound, it can

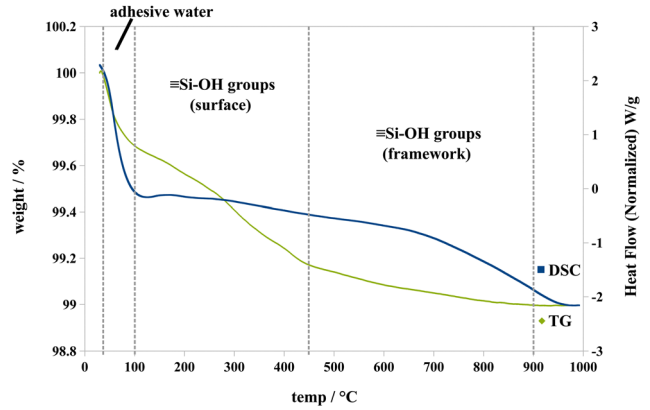

Fig. 3 DSC (blue) and TG (green) curves of as-made RUB-11.

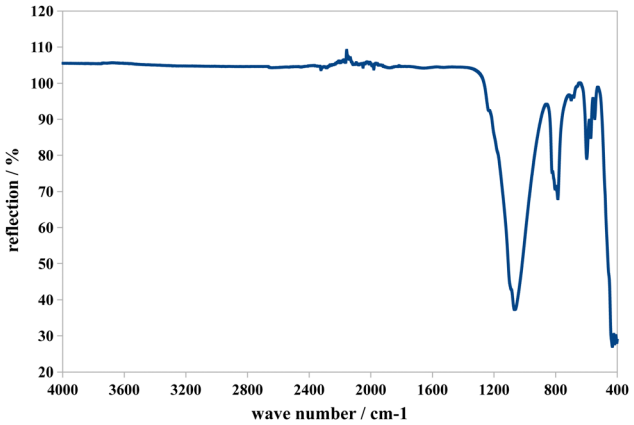

Fig. 4 (ATR)-FTIR spectrum of as-made RUB-11. The coarse background between 1900 and 2400 cm^{-1} is due to an incomplete compensation of the signals of the ATR crystal (diamond).

be assumed that RUB-11 possesses a pure silica framework. No further chemical analysis was performed.

Thermal analysis. The simultaneous DSC and TG analysis of as-made RUB-11 (Fig. 3) showed a very low total weight loss. In the range between 30 and 100 °C, a decrease of 0.31% is assigned to adhesive water. A second gradual weight loss between 100 °C and 450 °C of about 0.51% can be assigned to water generated from a small amount of ≡Si–OH groups. An additional very low weight loss of 0.18% occurs between 450 and 900 °C. The last two steps can tentatively be assigned to silanol groups at the surface of the plate-like crystals and isolated silanol defects of the framework, respectively. The generation of water from silanol groups corresponds to the small Q^3-type signal visible in the ^{29}Si NMR spectrum (see below).

The very low decrease in weight up to 450 °C proves that there are no free water molecules in the pore volume of RUB-11. Also, the presence of any organic material (ethylenediamine was part of the reaction mixture) in the structure can be excluded since no desorption is detected and no exothermic peak is visible, which would indicate a combustion of the organic material. The corresponding DSC curve is completely featureless without exo- or endothermal signals. The structure of RUB-11 is maintained after heating the sample up to 1000 °C as proven by a PXRD experiment (see Fig. S3, ESI†).

Infrared spectroscopy. The infrared spectrum (ATR-FTIR) of RUB-11 (Fig. 4) shows no signals at wavenumbers larger than 1300 cm^{-1}, indicating that RUB-11 does not contain any water, OH groups or organic species in detectable amounts. Bands in the silicate region between 350 and 1200 cm^{-1} are tentatively assigned as follows: the very broad band centered at 1066 cm^{-1} possessing a shoulder at 1094 cm^{-1} represents the asymmetric stretching vibration of Si–O–Si units. Another broad band centered at 804 cm^{-1} has some distinct "peaks" at 786 cm^{-1}, 804 cm^{-1} and 823 cm^{-1} and is assigned to symmetric stretching vibrations of the silica framework. The broad band around 410 cm^{-1} with small distinct "peaks" at 375 cm^{-1}, 394 cm^{-1}, 403 cm^{-1}, 416 cm^{-1} and 432 cm^{-1} represents the bending vibrations. Three bands at 546 cm^{-1}, 572 cm^{-1} and 598 cm^{-1} with very weak signals at 683 cm^{-1} and 699 cm^{-1} cannot be assigned to specific units of the structure. There is no band or shoulder visible at *ca.* 960 cm^{-1} which would indicate the presence of Si–OH groups; at this position, stretching vibrations of Si–OH groups typically occur. Although the structure of RUB-11 is quite complex and contains many symmetrically independent $SiO_{4/2}$-tetrahedra, only relatively few and broad FTIR signals are visible, indicative of a material with limited crystallinity. IR is a local probe. The broad signals are in agreement with $SiO_{4/2}$-tetrahedra with varying chemical environments. Fig. S4 (ESI†) presents a magnified view of the range from 350 to 1400 cm^{-1}.

NMR spectroscopy. The ^{29}Si MAS NMR spectrum (Fig. 5) presents three signals of the Q^4-type at −111.3 ppm, −114.7 ppm and −116.5 ppm, with relative intensities of 66%, 28% and 5%. A very small signal is visible at −106.4 ppm (Q^3-type, 1%) which is possibly caused by silanol units. Because of the pronounced plate-like morphology of the crystals, a significant part of the related signal may be due to terminal silanol groups at the large outer surface. Since the relaxation delay (T1) is very long for the impurity phase Xe-D3C, it does not contribute to the ^{29}Si signal.

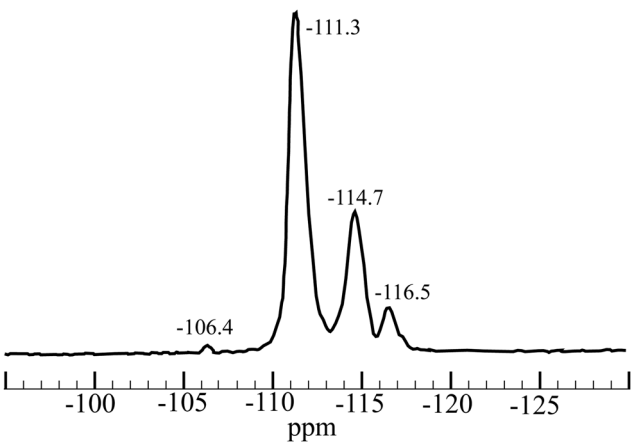

Fig. 5 ^{29}Si MAS NMR spectrum of RUB-11.

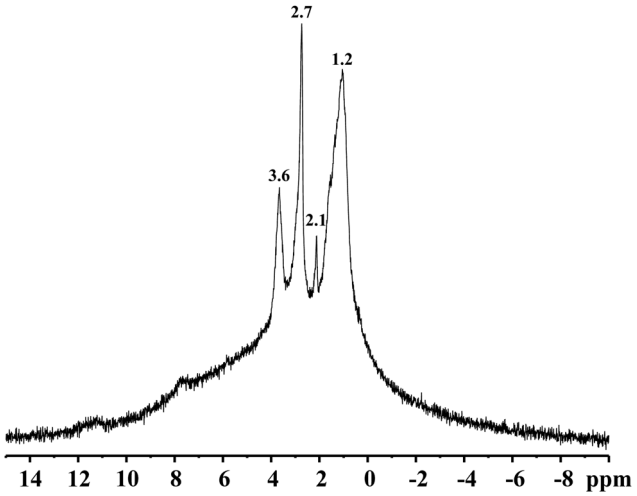

Fig. 6 ^{1}H MAS NMR spectrum of RUB-11.

The ^{1}H MAS NMR spectrum of RUB-11 (Fig. 6) displays only very weak signals. The two sharp signals at 2.7 ppm and 3.6 ppm are attributed to the organic compound (ethylenediamine) occluded together with xenon in the small Xe-D3C impurity. The signal at 2.7 ppm corresponds to the neutral ethylenediamine molecule,[33] while the signal at 3.6 ppm stems from protonated ethylenediamine.[34] A third, weak, broad and asymmetric signal around 1.2 ppm is assigned to OH groups being part of terminal silanol groups at the large outer surface of the RUB-11 crystals. The ^{1}H NMR spectrum is very much heightened, showing minor traces of the two organic compounds, which could not be detected by the DSC/TG and FTIR analyses.

Powder X-ray diffraction. The powder pattern of RUB-11 presents sharp and broadened reflections indicating a disordered structure. A detailed analysis of the half-widths is presented in Section 3.4.

Automatic indexing yielded a monoclinic unit cell as the most probable one with lattice parameters of a_0 = 7.39 Å, b_0 = 7.39 Å, c_0 = 26.05 Å and β = 98.2°. Unfortunately, it was not possible to determine the true space group symmetry of the structure based on the powder data. Thus, space groups *P*2, *Pm*, *P*2/*m*, *Pc*, *Pn*, *P*2/*c*, *P*2/*n*, *P*2$_1$/*c* and *P*2$_1$/*n* remained viable for the given choice of unit cell. Due to the obvious disorder, it was impossible to solve the structure of RUB-11 from the powder data.

Examining the porosity. Regrettably, the amount of sample was very limited and not sufficient for adsorption experiments since RUB-11 crystals (aggregates) had to be handpicked under the microscope. Instead, a comparison with RUB-5 may give a rough impression. The pore structure of RUB-11 is very similar to that of RUB-5,[11] both having a 2-dimensional pore system consisting of elliptical, intersecting 8-ring channels, which extend perpendicular to the *c*-axis. Free diameters of the channels are 3.2 × 4.6 Å and 3.8 × 4.2 Å for RUB-11 and RUB-5, respectively. Also, the densities are similar: 2.11 g cm^{-3} for RUB-11 and 2.20 g cm^{-3} for RUB-5. It can be expected that RUB-11 has approximately the same porosity as RUB-5 with a micropore volume of 0.057 cm^3 g^{-1} and a micropore surface of 210 m^2 g^{-1}.

3.3 Structure determination

3.3.1 Analysis of the average structure by 3D ED. One crystal has been measured with a very low total accumulated electron beam dose of approximately 9 e$^-$ Å^{-2} using PED. The reconstructed data revealed at first glance a primitive pseudo-tetragonal lattice (a_0 = 7.39 Å and c_0 = 51.8 Å) with very strong pronounced diffuse scattering parallel to the c*-axis. A closer look at the 3D ED data by taking the symmetry of the diffuse intensity distributions as the guideline revealed a primitive monoclinic lattice with the lattice parameters of a_0 = 7.3842 Å, b_0 = 7.3902 Å, c_0 = 26.1877 Å and β = 98.573°. The reconstructed observable reciprocal space showed sharp reflections perpendicular to the *c**-axis (Fig. 7a), again indicating that the structure is ordered well within the *ab*-plane. Electron diffraction also revealed systematic extinctions of the reflection class {*h*0*l*} with *l* = 2*n* + 1 (Fig. 7b), indicative of a *c*-glide plane and limiting the possible space group symmetries of the average structure to *Pc*, *P*2/*c* and *P*2$_1$/*c* (Laue class 2/*m*, $R_{\mathrm{int(obs)}}$ = 13.6%, 1343 observed reflections). A chemically reasonable structure model has been obtained using Direct Methods in the space group *Pc* with a residual value of $R_{1(\mathrm{obs})}$ = 24.8%. The unit cell contains 30 SiO_2 units connected by corner-sharing tetrahedra [$SiO_{4/2}$] as a structure motif. A dynamical refinement of the structure model was performed to obtain the optimised average structure. This converged to $R_{1(\mathrm{obs})}$ = 10.9%; further information on the dynamical refinement is summarised in Table S4 (ESI†). The dynamical refinement does not provide an unbiased structure model in this case, and, to avoid over-interpretation of the results, we refrain from a more detailed analysis and don't present atomic coordinates.

3.3.2 Rietveld refinement of the average structure. The structure refinement based on XRD powder data was performed to confirm the correctness of the average structure of RUB-11 by an independent method. The details of data collection and the results of the structure refinement are summarised in Table 2.

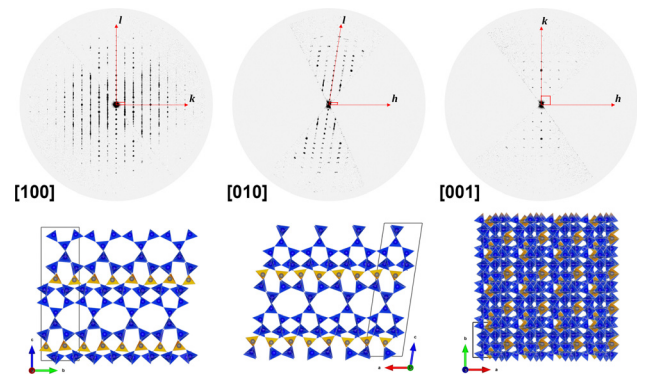

Fig. 7 Reconstructed reciprocal space sections (left) 0*kl*, (center) *h*0*l* and (right) *hk*0 recorded from a RUB-11 single crystal by 3D ED. The result of structure determination with view along [100], [010] and [001] plotted using VESTA.[32]

Table 2 Experimental and crystallographic parameters for the structure refinements of RUB-11

Diffractometer	Siemens D5000 with 6° PSD
Wavelength	1.54059 Å
Sample	0.3 mm glass capillary
2θ range of data used [°]	5.0–90.0
Step size [° 2θ]	0.00790
No. steps	10754
No. contributing reflections	1296
No. geometric restraints	180
No. structural parameters	134
No. profile parameters	21
FWHM[a] in the range 23–26° 2θ	0.10–0.66
R_{Bragg}	0.043
R_{wp}	0.069
R_{exp}	0.018
χ^2	14.3
Space group	*Pc* (No. 7)
a_0 [Å]	7.3929(5)
b_0 [Å]	7.3942(3)
c_0 [Å]	26.1786(13)
β [°]	98.372(7)
VUC [Å^3]	1415.8(1)
Density (calc.) [g cm^{-3}]	2.114
Unit cell content	$Si_{30}O_{60}$

[a] FWHM of reflexions (114), (016), (020), ($\bar{2}$02), (021), (200), (022), ($\bar{1}$16), (106), and (115).

The refinement finally converged to R_{Bragg} = 0.043 and R_F = 0.037. Because of the disorder, which generates both sharp and broad reflections, the profile fit remained unsatisfactory with a χ^2 value of 14.3 (see also Fig. 8).

The X-ray powder diagram (see Fig. 8) presents a mixture of moderately sharp and broadened reflections. Nevertheless, all reflections have been indexed based on a monoclinic lattice.

3.3.3 DLS refinements. A distance-least-squares refinement using the DLS-76 program[28] was conducted to verify the physical feasibility of a SiO_2 framework possessing the RUB-11 structure. The refinement converged to an excellent *R*-value of 0.0040 for an optimised structure with Si–O bond lengths in the range of 1.6035–1.6116 Å, Si···Si distances in the range of 2.9878–3.1692 Å and O···O distances in the range of 2.6073–2.6438 Å. This confirms that a relaxed SiO_2-framework possessing the topology of the RUB-11 structure is possible. The optimised atomic coordinates are listed in Table S3 (ESI†).

Table S6 (ESI†) displays a distance-least-squares refinement of hypothetical endmember B of the RUB-11 framework structure.

3.3.4 Description of the average structure. There are 15 symmetrically independent silicon atoms and 30 independent oxygen atoms in the structure (see Table S4, ESI†). According to the Rietveld refinement, the distances between atoms are listed

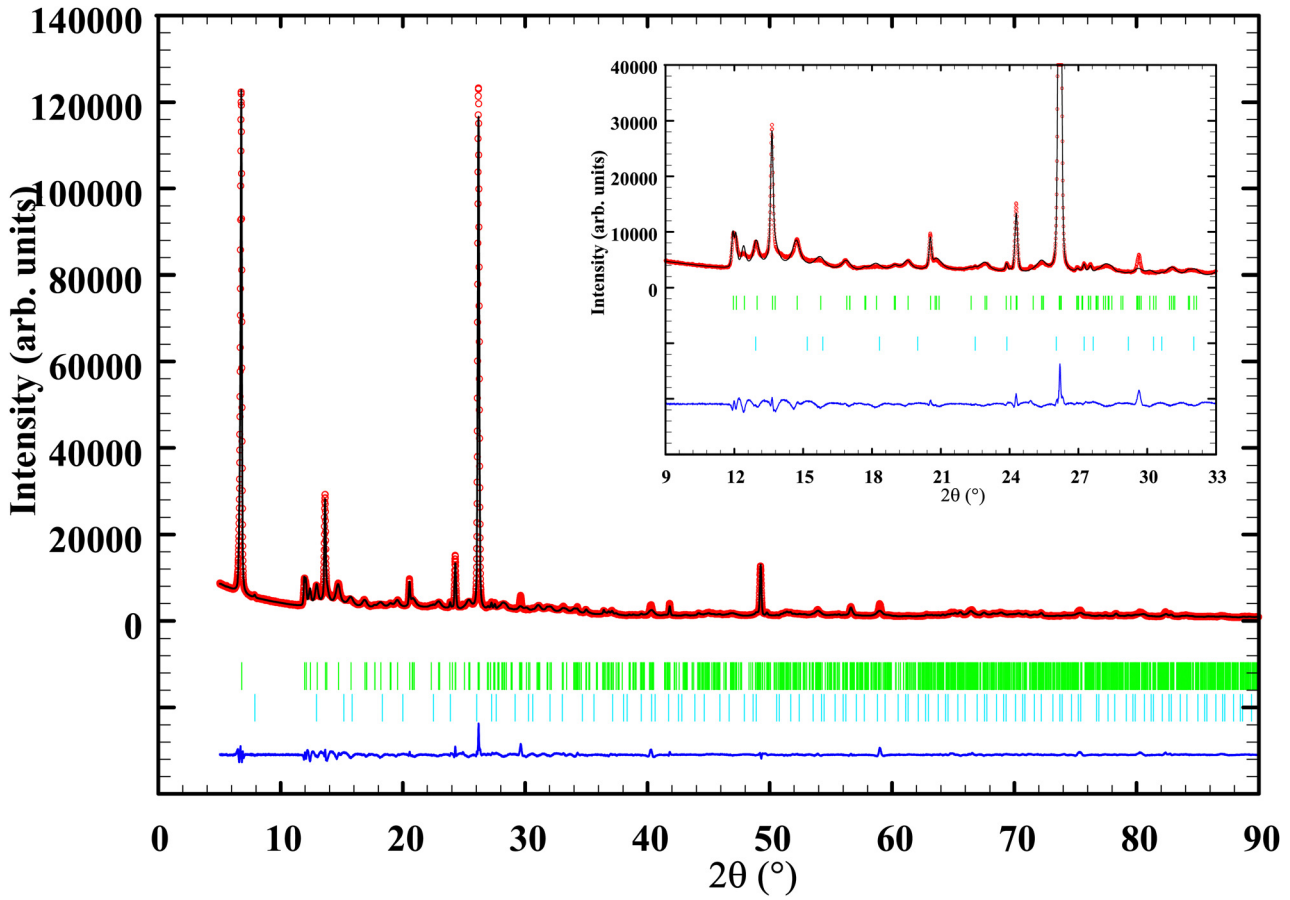

Fig. 8 Plot of the Rietveld analysis of RUB-11. Experimental data (red) and calculated data (black) are in the upper trace, and the difference plot (blue) is shown below. Tick marks indicate the allowed reflections of RUB-11 (upper trace, green) and MTN-type zeolites (lower trace, teal).

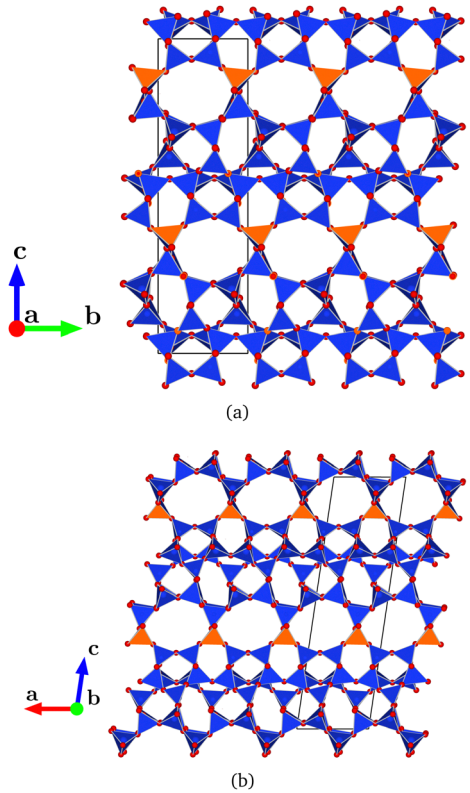

Fig. 9 The average structure of RUB-11 in two projections. Blue tetrahedra represent the magadiite-type layers while orange tetrahedra represent the interconnecting building units creating a 3D zeolite framework. Plotted using VESTA.[32]

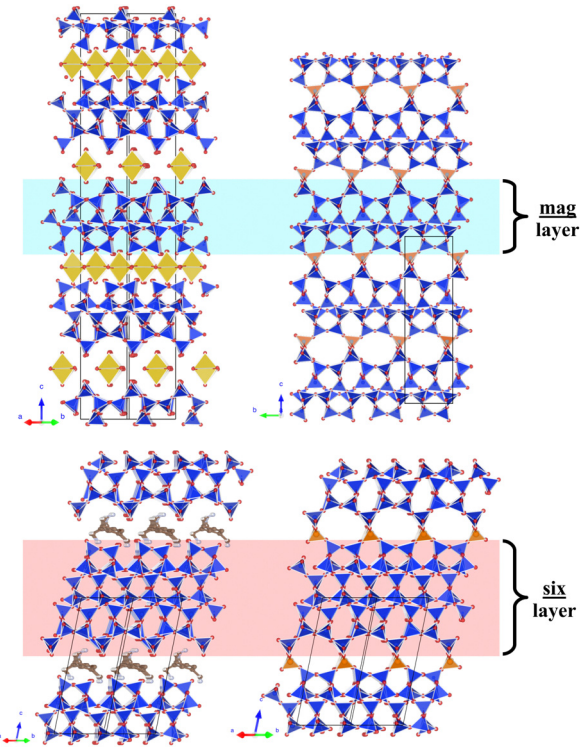

Fig. 10 Comparison of the structures of layer silicate magadiite (upper left) and the corresponding IEZ RUB-11 (upper right), as well as the layer silicate RUB-6 (lower left) and the corresponding IEZ RUB-5 (lower right). The mag layers of magadiite and RUB-11, and the six layers of RUB-6 and RUB-5 are shown as blue tetrahedra, while the interconnecting tetrahedra of the IEZ structures (right hand side) are displayed in orange. Plotted using VESTA.[32]

in the ranges of d(Si–O) = 1.55(9)–1.65(6) Å, d(Si···Si) = 2.99(6)–3.16(6) Å, and d(O···O) = 2.37(8)–2.77(10) Å. The unit cell content of RUB-11, with respect to the structural and chemical analyses, is $[Si_{30}O_{60}]$.

The structure of RUB-11 consists of interconnected layer-like building units with a thickness of 12.95 Å (two per unit cell). These LLBUs can be deconstructed into two parts: (i) dense magadiite type layers (mag layers) made up of 4-, 5-, 6- and 7-rings with a nominal composition of $[Si_{14}O_{28}]$ per 2-dim. unit cell and (ii) an additional tetrahedrally coordinated silicon atom on top of the layer (Fig. 9a). The mag layers are stacked along the c-axis and are interconnected to each other by these $[Si_{4/2}]$ tetrahedra (two 4-connected tetrahedra per unit cell) forming a microporous framework (see Fig. 9b). The insertion of the additional tetrahedra between mag layers in the RUB-11 framework leads to the formation of a 2-dimensional pore system of intersecting 8-ring channels (with free diameters of 3.2 × 4.6 Å) extending perpendicular to the c-axis.

Compared to magadiite possessing an ABCDABCD... stacking sequence of mag layers, the sequence in RUB-11 is ABAB... (see Fig. 10). It is interesting to note that the mag layers of magadiite can directly be interconnected to each other by a condensation reaction without additional SiO_4 tetrahedra. Replacing the hydrated sodium cations by suitable organic molecules, it is possible to form a high density zeolite with 8-ring channels named RWZ-1.[35]

RUB-11 is a zeolite of very high density and has a framework density of FD = 21.2, which is identical to the one of chiral zinc phosphate (code CZP, FD = 21.2),[5] the zeolite type of the highest framework density, so far (FD: number of tetrahedra per 1000 Å^3).

3.3.5 Comparison with structurally related materials (layer silicates magadiite and RUB-6, and framework silicate RUB-5). Magadiite is a layered sodium silicate consisting of thick silicate layers and intercalated bands of edge-sharing $[Na(H_2O)_{6/1.5}]$ octahedra (Fig. 10).[36,37]

RUB-11, however, crystallises directly from its reaction mixture during the hydrothermal synthesis with a quite long reaction time. It is surprising that the channel-like pores of RUB-11 are completely empty when separated from the reaction mixture.

The plate-like morphology of crystals suggests that RUB-11 possibly forms *via* a layered intermediate, which, in the late stage of the synthesis run, is intercalated by additional silicic acid available in the reaction mixture. A condensation process involving the silanol groups of the silicate layers and monomeric silicic acid may finally generate the framework of RUB-11. Using this type of reaction, several microporous materials have been obtained by Ikeda *et al.*[37] So called "pillared lamellar silicates", named APZ-1, APZ-2, APZ-3 and APZ-4, were

prepared by thermal acid treatment of the layered silicates PLS-1, PLS-3, PLS-4, and PREFER, which consist of ferrierite type silicate layers. These layer silicates could be converted into APZ materials representing new open-framework microporous materials by pillaring with $SiO_2(–OH)_2$ fragments. While the APZ and IEZ materials possess interrupted frameworks, RUB-11 has a fully 4-connected silica framework. IEZ materials may be generated by one of three procedures, either in a two-step process with MeX4, in a two-step process of self-pillaring or in a one-step synthesis, as is the case for RUB-11 or RUB-5.

A similar relationship exists between the zeolite-like framework silicate RUB-5 and the layer silicate RUB-6, both containing the same dense layers designated as the type six layer.[38] Whilst these layers are terminated by silanol/siloxy groups and separated from each other in RUB-6, in RUB-5, the layers are fully interconnected by additional, tetrahedrally coordinated silicon atoms forming a silicanon-interrupted framework. This framework has a 2D pore system consisting of intersecting 8-ring channels.[10,11] RUB-5 can be regarded as an IEZ based on the silicate layers of RUB-6. It is interesting to note that the as-made RUB-5 has – like RUB-11 – a pronounced plate-like morphology and crystallises with an empty pore system. It was assumed that the materials of the phyllo/tectopair RUB-6 and RUB-5 form sequentially (in the given reaction mixture) with the first formation of the layer; and a second 3D interconnecting process, either leading to the crystallisation of layered RUB-6, if a suitable cation is available in the reaction mixture to compensate the charge of the layer, or the crystallisation of the framework silicate RUB-5, if no suitable organic compound is accessible. In the second case, a condensation reaction is assumed involving the silanol/siloxy groups of neighbouring silicate layers and additional $Si(OH)_4$ tetrahedra from the remaining reaction mixture. A similar relationship is proposed here for layer silicate magadiite and the title compound RUB-11.

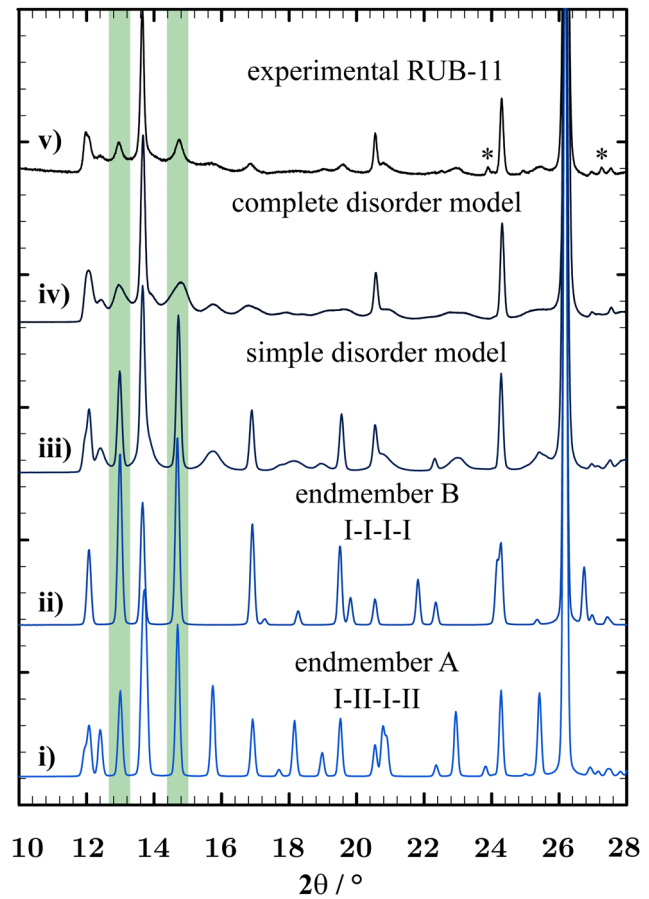

Fig. 11 Section of simulated PXRD diagrams of (i) endmember A – the average structure (I-II-I-II-), (ii) endmember B – an idealised structure of only one LLBU (I-I-I-I-), (iii) a random mixture of all three endmembers A, B and C and (iv) the optimised disordered structure involving the average structure in combination with sequences of endmembers B and C and interjections of LLBUs rotated by 180° and (v) the experimental PXRD diagram of RUB-11 (the impurity phase of D3C is marked with an asterisk) (from bottom to top). Highlighted in green at about 13.1° 2θ and 14.6° 2θ are two reflections particularly sensitive to layer disorder.

3.4 Analysis of the real structure

The layers of RUB-11 are stacked perpendicular to the *ab*-plane. In order to understand the contribution of disorder to the powder pattern, it is instructive to compare the half-widths of specific reflections. All reflections *hkl* with indices $h \neq 0$, $k \neq 0$

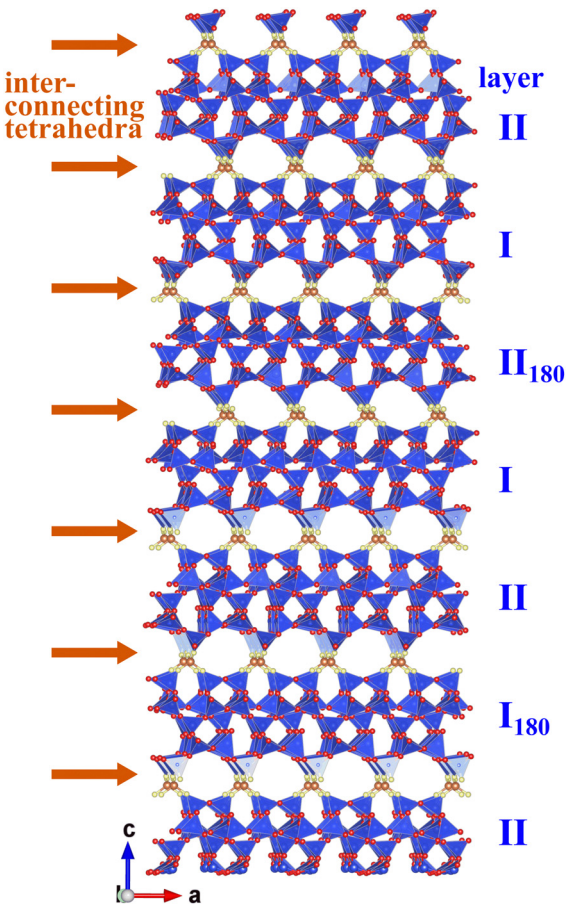

Fig. 12 Sequence of different layers highlighting all possible types of interconnections. Plotted using VESTA.[32]

and $l \neq 0$ are broad while $hk0$ reflections are sharp. The sharpness of the $hk0$-reflections indicates that the structure is ordered well within the layer-like building unit (*ab*-plane). The fact that $00l$-reflections are also reasonably sharp (although the thickness of the crystals is only about 0.1 μm) indicates that the repeat unit along the stacking direction of LLBUs (*c*-axis) is identical throughout the crystal.

The regular (average) structure of RUB-11 with an ordered I-II-I-II-... stacking sequence (endmember A) is similar to the structure of magadiite which, however, contains separated (mag) layers instead of the closely related, interconnected building units I and II of RUB-11.

Although the average structure dominates the stacking sequence of the real structure, considerable disorder is observed. The type of stacking disorder was investigated in detail by calculating hypothetical powder diagrams corresponding to various stacking sequences. Since the ^{29}Si NMR spectrum (and the refinements of the average structure) proved that RUB-11 has a fully 4-connected framework, only specific relative layer arrangements are possible, which allow for a complete interconnection to generate a framework without "dangling bonds". This limitation still admits that not only a replacement of a given LLBU by another LLBU (I ⇔ II) is possible, but that it is also viable to rotate the LLBUs by 180° about the stacking direction, generating additional LLBUs I_{180} and II_{180}.

Fig. 11 shows a comparison of XRD powder diagrams of the experimental powder pattern and some relevant simulated structure models (the impurity phase D3C is not taken into account for the simulations). The random addition of monotonous I-I (endmember B) and II-II (endmember C) sequences to the average structure (I-II-I-II-... – endmember A) illustrates one type of disorder. Endmembers B and C are enantiomorphic structures and generate the same PXRD pattern. They possess space group symmetry *C*2. An exemplary stacking sequence of the disordered RUB-11 framework would present as follows: I-II-I-II-I-I-I-II-I-II-II-I (a mixture of endmembers A, B and C representing a basic disorder type). A distance-least-squares refinement of endmember B (*R*-value: 0.0036) proved that a I-I-I-... stacking would generate a regular SiO_2 framework with Si–O bond lengths in the range of 1.598 Å to 1.602 Å, Si···Si distances in the range of 2.997 Å to 3.137 Å and O···O distances in the range of 2.590 Å to 2.642 Å (see Table S6, ESI†). The fact that both endmembers A (I-II-I-II-...) and B (I-I-I-...) can form relaxed frameworks without distortion is probably the reason that RUB-11 crystallises with a random stacking of LLBUs.

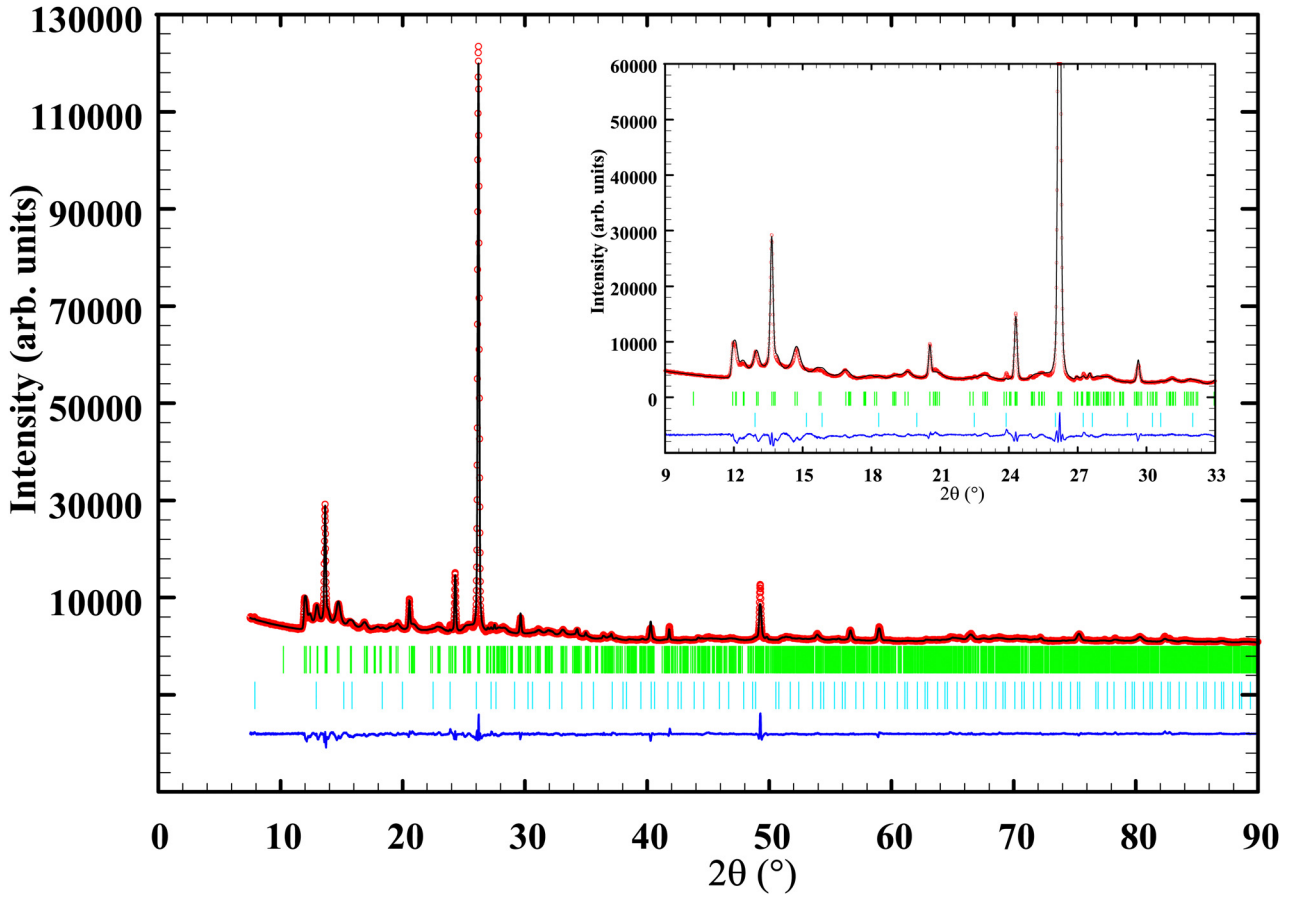

Fig. 13 PXRD patterns of the FAULTS refined disorder model (black) compared to the experimental data (red) with allowed reflections as green ticks (upper line) for the average RUB-11 structure and the teal ticks (lower line) for the impurity phase D3C, as well as the difference curve in blue. The first reflection was excluded because the pronounced asymmetry cannot be accounted for by the FAULTS program.

While this model comes already close to the real structure, another type of disorder is necessary for a complete description of the real structure. The addition of rotated layers I_{180} and II_{180} to the pattern yields a structure model that fits the experimental PXRD curve best. A combination of about 65% of the average structure (endmember A), 3.5% of I–I (endmember B) plus 3.5% of II-II (endmember C) sequences, and the addition of isolated I_{180} and II_{180} layers (14% and 14%, respectively) induces the best correspondence to the experimental powder pattern of RUB-11 and served as a starting model for the FAULTS refinement. Fig. S5 in the ESI† illustrates the starting model in comparison with the experimental PXRD pattern and the resulting complete disorder model. Fig. S6 (ESI†) displays all four types of mag layers adopted in the RUB-11 framework structure.

Fig. 12 presents a specific sequence of different layers including all possible types of interconnections. It is obvious that the layers can be linked to each other without ''dangling bonds'' and without noticeable distortion.

The average model, the simple disorder model and the resulting optimised model are shown in Fig. S7 in the ESI.†

Similar to the classical Rietveld refinement, the FAULTS refinement included the optimisation of the global parameter zero-shift, scale factors for RUB-11 and impurity phase D3C, pseudo-Voight profile parameters u, v, w and x, and the lattice parameters excluding the angles defining the stacking direction.

Additionally, the FAULTS-specific algorithm admits the refinement of transition probabilities and shift vectors. The former describes the probability of a specific type of LLBU being stacked on the previous LLBU (in %). The latter specifies the position of a succeeding LLBU in relation to the previous LLBU, which is defined as the shift vector with fractional values of x, y and z. A complete description of the refined values is found in Table S2 in the ESI.†

Fig. 13 shows the simulated disorder model of the refinement to the experimental PXRD data using FAULTS.[31] The visualisation occurs in the style of the Rietveld Refinement using the program FullProf.[27] Due to the disorder, no definite Bragg reflections of RUB-11 can be shown in the graphics. However, the program allows for a visual aid by displaying Bragg reflections of the average structure of RUB-11. The refinement yielded residue values of $\chi^2 = 7.1$ and $R_F = 4.0$, thus, improving the Rietveld refinement by a factor of 2 (even without accounting for the peak asymmetry). Transition probabilities converged to 54.5% for the average structure (endmember A), 13% for the I-I transition (endmember B), 8.1% for the II-II transition (endmember C), 8.8% for transition II-I_{180}-II and 13.0% for transition I-II_{180}-I.

The probabilities for each transition (Fig. S8, ESI†) in conjunction with a more detailed overview of transition probabilities and vectors (Table S2, ESI†) can be found in the ESI.†

FAULTS also allows the calculation of the selected area electron diffraction (SAED) patterns, which can be compared to the corresponding ones of the electron diffraction. Fig. 14 displays a comparison of such SAEDs 0*kl* (top left) and *h*0*l* (bottom left) calculated for the average structure compared to the experimental ED data (middle), as well as the SAED patterns of the disordered structure (right) as derived from the FAULTS refinement.

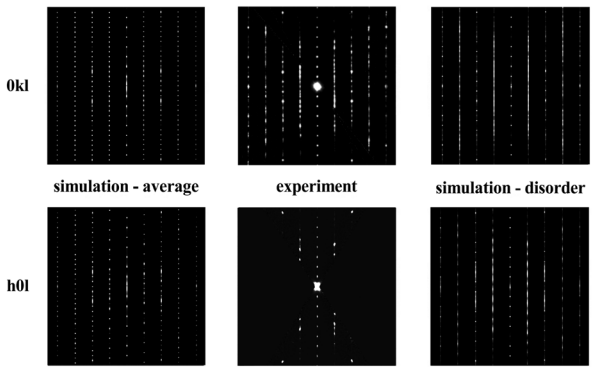

Fig. 14 Comparison of selected area electron diffraction (SAED) patterns of 0*kl* and *h*0*l* sections for the calculated average structure (left), the experimental data (middle) and the simulated disordered (real) structure derived from the FAULTS refinement.

4 Conclusions

The all-silica, high-density zeolite RUB-11 has been obtained using a one-step hydrothermal synthesis method over very long reaction times. Due to the small crystal size, the complex structure and the severe disorder (observed both by PXRD and electron diffraction data), the structure could only be solved by electron diffraction experiments. The knowledge of the recently solved structure of the layer silicate magadiite constructed from thick, dense silicate layers, referred to as mag layers, was helpful to assign atoms to the experimentally obtained potential map. The refinement of the average structure against electron diffraction data and PXRD data combined with a distance-least-squares refinement of the hypothetical ordered framework confirms the structure model of RUB-11. Magadiite and RUB-11 are closely related structurally, containing the same silicate layers. In the case of RUB-11, these (mag) layers are connected to each other *via* an additional silicon atom. RUB-11 can, therefore, formally be regarded as the interlayer expanded zeolite (IEZ) of magadiite. Different from other IEZs, which usually are synthesised in a two-step process, RUB-11 has a fully 4-connected framework with a 2-dimensional pore system consisting of intersecting 8-ring channels.

A certain degree of stacking disorder is a common feature of hydrous layered silicates and interlayer expanded materials. RUB-11, however, displays a much higher degree of disorder than, for example, the related layer silicate magadiite. While the mag layers are fairly ordered within the *ab*-plane, the disordered stacking of the layers is responsible for the reduced quality of diffraction data exhibiting many very broad reflections. The analysis of the nature of the disorder led to a deeper insight into the complex real structure of RUB-11. The program

FAULTS allowed for a refinement (against experimental PXRD data) of shift vectors between successive layers, profile parameters and the percentage of the different structural motives making up the real structure of RUB-11. Ultimately, two different disorder models had to be considered to adequately describe the real structure of RUB-11, all the while keeping individual layers fully connected. The disorder includes a random stacking of the enantiomorphic LLBUs I and II, as well as the random interjection of additional LLBUs I_{180} and II_{180}, which are rotated by 180° about the stacking direction. Only about 54.5% of the real structure refers to the ordered end-member A, which is identical to the average structure. The simulation of selected area diffraction patterns and comparison with experimental electron diffraction data confirmed these findings. Topologically, the disordered RUB-11 framework reveals a non-blocked pore-system of intersecting 8-ring channels.

Unexpectedly, the pore system of as-obtained RUB-11 is free of extra-framework species, in particular free of water, although crystallising from an aqueous solution. This has also been observed for a related material, RUB-5,[11] which can be regarded as the IEZ of layer silicate RUB-6. RUB-11, RUB-5 and condensed magadiite[35] are small pore zeolites which are hydrophobic and chemically and thermally very stable and possess an unusual high density but are still porous. These features may constitute a significant potential for specific industrial applications.

Author contributions

Isabel Grosskreuz: investigation, formal analysis and writing – original draft; Yasar Krysiak: investigation and formal analysis; Hermann Gies: conceptualisation and validation; Enrico Mugnaioli: investigation; Bernd Marler: investigation, project administration, writing – review and editing, and funding acquisition.

Conflicts of interest

There are no conflicts to declare.

Acknowledgements

The authors thank anonymous reviewers for helpful comments to improve the manuscript. This work was financially supported by the Deutsche Forschungsgemeinschaft (Projekt MA 6641/3-1) and the authors thank Dr Ute Kolb, Mainz, Germany, for instructive discussions.

Notes and references

1 F. R. Ribeiro, Zeolites, science and technology: [Proceedings of the NATO Advanced Study Inst. on 'Zeolites, Science and Technology', Alcabideche, Portugal, May 1–12, 1983.] ed. Fernando Ramôa Ribeiro [a.o.], Nijhoff, The Hague usw., 1984, vol. Ser. (E, 80).
2 C. J. Rhodes, *Sci. Progress*, 2010, **93**, 223–284.
3 *Catalysis, green chemistry and sustainable energy: New technologies for novel business opportunities*, ed. A. Basile, G. Centi, M. D. Falco and G. Iaquaniello, Elsevier, Amsterdam, Netherlands and Cambridge, MA, 2020, vol. 179.
4 C. Baerlocher, D. H. Olson, L. B. McCusker and W. M. Meier, *Atlas of zeolite framework types*, Published on behalf of the Structure Commission of the International Zeolite Association by Elsevier, Amsterdam and Boston, 6th edn, 2007.
5 C. Baerlocher and L. B. McCusker, *Database of Zeolite Structures*, 2017, **https://www.iza-structure.org/databases/**.
6 S. Inagaki, T. Yokoi, Y. Kubota and T. Tatsumi, *Chem. Commun.*, 2007, 5188–5190.
7 P. Wu, J. Ruan, L. Wang, L. Wu, Y. Wang, Y. Liu, W. Fan, M. He, O. Terasaki and T. Tatsumi, *J. Am. Chem. Soc.*, 2008, **130**, 8178–8187.
8 S. Inagaki, H. Imai, S. Tsujiuchi, H. Yakushiji, T. Yokoi and T. Tatsumi, *Microporous Mesoporous Mater.*, 2011, **142**, 354–362.
9 T. De Baerdemaeker, W. Vandebroeck, H. Gies, B. Yilmaz, U. Müller, M. Feyen and D. E. de Vos, *Catal. Today*, 2014, **235**, 169–175.
10 Y. Krysiak, B. Marler, B. Barton, S. Plana-Ruiz, H. Gies, R. B. Neder and U. Kolb, *IUCrJ*, 2020, **7**, 522–534.
11 B. Marler, Y. Krysiak, U. Kolb, C. Grafweg and H. Gies, *Microporous Mesoporous Mater.*, 2020, **296**, 109981.
12 B. Marler, A. Grünewald-Lüke, T. Ikeda, P. Zuber, H. Heimes and H. Gies, *Database of Hydrous Layer Silicates*, 2019, **https://hls-database.com/**.
13 J. M. Newsam, M. M. J. Treacy, W. T. Koetsier and C. B. D. Gruyter, *Proc. R. Soc. London, Ser. A*, 1988, **420**, 375–405.
14 J. B. Higgins, R. B. LaPierre, J. L. Schlenker, A. C. Rohrman, J. D. Wood, G. T. Kerr and W. J. Rohrbaugh, *Zeolites*, 1988, **8**, 446–452.
15 J. Ruan, P. Wu, B. Slater, Z. Zhao, L. Wu and O. Terasaki, *Chem. Mater.*, 2009, **21**, 2904–2911.
16 H. Gies, U. Müller, B. Yilmaz, T. Tatsumi, B. Xie, F.-S. Xiao, X. Bao, W. Zhang and D. E. de Vos, *Chem. Mater.*, 2011, **23**, 2545–2554.
17 T. Ikeda, S. Kayamori, Y. Oumi and F. Mizukami, *J. Phys. Chem. C*, 2010, **114**, 3466–3476.
18 Y. Asakura, R. Takayama, T. Shibue and K. Kuroda, *Chem. – Eur. J.*, 2014, **20**, 1893–1900.
19 S. Vortmann, Diploma thesis, Ruhr-University Bochum, Bochum, 1994.
20 S. Plana-Ruiz, Y. Krysiak, J. Portillo, E. Alig, S. Estradé, F. Peiró and U. Kolb, *Ultramicroscopy*, 2020, **211**, 112951.
21 R. Vincent and P. A. Midgley, *Ultramicroscopy*, 1994, **53**, 271–282.
22 E. Mugnaioli, T. E. Gorelik and U. Kolb, *Ultramicroscopy*, 2009, **109**, 758–765.
23 L. Palatinus, *PETS: program for analysis of electron diffraction data*, 2011.

24 M. C. Burla, R. Caliandro, B. Carrozzini, G. L. Cascarano, C. Cuocci, C. Giacovazzo, M. Mallamo, A. Mazzone and G. Polidori, *J. Appl. Crystallogr.*, 2015, **48**, 306–309.
25 P. A. Doyle and P. S. Turner, *Acta Crystallogr., Sect. A*, 1968, **24**, 390–397.
26 V. Petříček, M. Dušek and L. Palatinus, *Z. Kristallogr. - Cryst. Mater.*, 2014, **229**, 345–352.
27 J. Rodríguez-Carvajal, *Commission on Powder Diffraction (IUCr)*, 2001, **Newsletter No. 26** (December) pp. 12–19.
28 C. Baerlocher, A. Hepp and W. M. Meier, DLS-76, a FORTRAN program for the simulation of crystal structures by geometric refinement, 1978, **https://www.crystal.mat.ethz.ch/Software/**.
29 M. M. J. Treacy, M. W. Deem and J. M. Newsam, DIFFaX, 2010, **https://www.public.asu.edu/mtreacy/DIFFaX.html**.
30 H. Grell, C. Krause and J. Grell, *Tables of the 80 plane space groups in three dimensions*, Institut für Informatik und Rechentechnik, Akademie der Wissenschaften der DDR, 1988.
31 M. Casas-Cabanas, M. Reynaud, J. Rikarte, P. Horbach and J. Rodríguez-Carvajal, *J. Appl. Crystallogr.*, 2016, **49**, 2259–2269.
32 K. Momma and F. Izumi, *J. Appl. Crystallogr.*, 2011, **44**, 1272–1276.
33 Chemical Book, Ethylenediamine dihydrochloride: CAS333-18-6, 2017, **https://www.chemicalbook.com/SpectrumEN_333-18-6_1HNMR.htm**.
34 Chemical Book, Ethylenediamine: CAS107-15-3, 2017, **https://www.chemicalbook.com/SpectrumEN_107-15-3_1HNMR.htm**.
35 M. Koike, I. Grosskreuz, Y. Asakura, R. Miyawaki, H. Gies, H. Wada, A. Shimojima, B. Marler and K. Kuroda, *Chem. – Eur. J.*, 2023, e202301942.
36 Y. Krysiak, M. Maslyk, B. N. Silva, S. Plana-Ruiz, H. M. Moura, E. O. Munsignatti, V. S. Vaiss, U. Kolb, W. Tremel, L. Palatinus, A. A. Leitão, B. Marler and H. O. Pastore, *Chem. Mater.*, 2021, **33**, 3209–3219.
37 B. Marler, Y. Krysiak, I. Grosskreuz, H. Gies and U. Kolb, *Am. Mineral.*, 2022, **107**, 2101–2110.
38 H. Gies, U. Müller, B. Yilmaz, M. Feyen, T. Tatsumi, H. Imai, H. Zhang, B. Xie, F.-S. Xiao, X. Bao, W. Zhang, T. De Baerdemaeker and D. E. de Vos, *Chem. Mater.*, 2012, **24**, 1536–1545.

